Cellular & Molecular Intelligence, Vol. 1, No. 1, pp. 1000–1025, 2026

OPEN ACCESS https://doi.org/10.22201/ia.01851101p.20XX.XX.XX.XX

Computational and Biophysical Characterization of Limonene as a Potential Natural Inhibitor of CDK6 for Therapeutic Targeting of Cancer

Zulfareen[1,*], **Sumra**[2] **and Shagufta Jahan**[1]

[1]*Centre for Interdisciplinary Research in Basic Sciences, Jamia Millia Islamia, Jamia Nagar, New Delhi 110025, India*
[2]*Department of Biotechnology, Jamia Millia Islamia, Jamia Nagar, New Delhi 110025, India*
[*]*Correspondence: zulfareengaur@gmail.com*

Abstract

Cyclin-dependent kinase 6 (CDK6) plays a central role in G1–S phase cell cycle progression and is frequently dysregulated in various cancers, making it an established therapeutic target. Although selective CDK4/6 inhibitors are clinically available, exploration of natural compounds targeting CDK6 remains limited. The present study aimed to investigate the binding mechanism and inhibitory potential of limonene against CDK6 using integrated computational and experimental approaches. Recombinant CDK6 was cloned, expressed, and purified, followed by molecular docking, fluorescence spectroscopy, and kinase inhibition assay. Docking analysis revealed a binding free energy of -6.3 kcal mol^{-1} with a calculated pK_i of 4.62 and ligand efficiency of 0.63 kcal mol^{-1} per non-hydrogen atom. Fluorescence quenching studies demonstrated strong binding affinity ($K = 4.1\times10^7$ M^{-1}), while enzymatic assays confirmed dose-dependent suppression of CDK6 activity. Collectively, these findings indicate that limonene directly interacts with and functionally inhibits CDK6, highlighting its potential as a natural scaffold for the development of CDK6-targeted anticancer therapeutics.

Keywords: *Cyclin-dependent kinase 6, Limonene, Molecular docking, Fluorescence spectroscopy, Kinase inhibition assay, Proteinligand interaction, Cell cycle regulation, Anticancer therapy*

Received: April 16th, 2024 **Accepted:** March 21th, 2024 **Published:** March 31, 2026

1. INTRODUCTION

Cancer is characterised by uncontrolled cell proliferation, driven largely by dysregulation of the cell cycle. The cell cycle comprises a series of phases, and key regulators include cyclins, cyclin-dependent kinases (CDKs), and CDK inhibitors (CKIs), which work together to control progression through these phases. The disruption of these components of the cell cycle is a core hallmark of cancer, enabling uncontrolled cell proliferation and tumorigenesis (Hanahan & Weinberg, 2011; **?**).

Cyclin-dependent kinases (CDKs) are serine/threonine protein kinases that are involved in the cell cycle, transcription, and other biological processes like translation, neurogenesis, and apoptosis (Malumbres, 2014). Among CDK family members, cyclin-dependent kinase-6 (CDK6) and CDK4 play important roles in mammalian cell proliferation by driving cells into the DNA synthetic (S) phase of the cell division cycle (Sherr et al., 2016). CDK4 and CDK6 associate with D-type cyclins (D1, D2, and D3), which phosphorylate retinoblastoma (RB), thereby releasing E2F transcription factors. E2F-dependent gene activation allows for G1 to S phase progression and DNA synthesis (Classon & Harlow, 2002), helping cells progress through the early G1 phase of the cell cycle (Nebenfuehr et al., 2020). Beyond its function in cell cycle control, CDK6 contributes to cell differentiation, tissue development, and hematopoietic lineage commitment (Tigan et al., 2016). Emerging evidence also suggests that CDK6 modulates anti-tumour immunity by regulating immune cell proliferation and immune checkpoint molecule expression (Petroni et al., 2020). Figure 1 illustrates the transcriptional, post-transcriptional, and post-translational regulation of Cyclin D–CDK4/6.

CDK6 and CDK4 form larger protein complexes with heat shock protein 90 (Hsp90) and its co-chaperone cell division cycle 37 (Cdc37), which secure correct protein folding, assembly, maturation, and stability of a large number of proteins (Hallett et al., 2017). Hyperactivation of CDK6 has been linked to various malignancies, including breast cancer, leukaemia, lymphoma, and glioblastoma. Experimental disruption of CDK6 prolongs the G1 phase and inhibits S-phase entry. G1-phase prolongation causes premature differentiation in neuroepithelial cells, which explains reduced proliferation after CDK6 loss (O'Sullivan, 2026).

Structurally, CDK6 is a 326-amino-acid protein (~36.5 kDa) encoded on chromosome 7 (Russo et al., 1998). It comprises several key domains: the N-terminal lobe (residues 1–98) contains a regulatory cyclin-binding domain, while the C-terminal lobe forms the catalytic core (Sielecki et al., 2000). The activation (T-) loop (residues 156–172) within the catalytic domain regulates kinase activity through phosphorylation, while additional regulatory motifs, including a C-terminal PEST sequence, contribute to protein stability (Li et al., 2015).

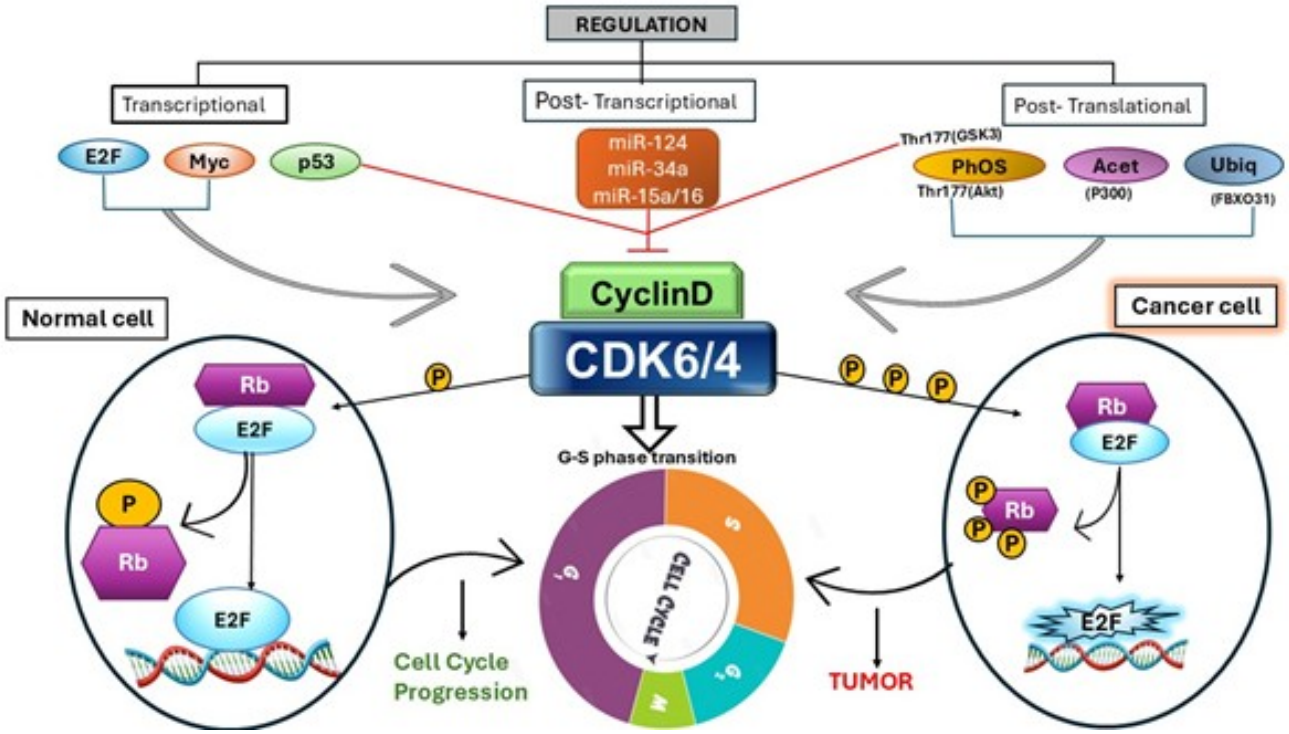

Figure 1. The schematic illustration of transcriptional, post-transcriptional, and post-translational regulation of Cyclin D–CDK4/6. In normal cells, controlled CDK4/6 activation leads to the regulated phosphorylation of the retinoblastoma protein (Rb), releasing E2F to permit orderly G1–S progression. In contrast, hyperactivation of CDK4/6 in cancer cells leads to excessive Rb phosphorylation, sustained E2F hyperactivation, and uncontrolled cell cycle progression, contributing to tumor development.

Activation of CDK6 requires interaction with cyclin D and phosphorylation by CDK-activating kinase (CAK), whereas its activity is negatively controlled by INK4 and Cip/Kip family inhibitors. Beyond phosphorylation, CDK6 is finely regulated at transcriptional, post-transcriptional (e.g., microRNAs such as miR-124 and miR-34a), and post-translational levels, including phosphorylation, acetylation, and ubiquitination (Bachs et al., 2018; Garzon et al., 2010).

Due to its primary function in tumour growth and survival, CDK6 has been recognised as a validated therapeutic target (Yousuf et al., 2022). Selective CDK4/6 inhibitors, Palbociclib, Ribociclib, and Abemaciclib, have shown considerable clinical benefit and have been approved by regulators for hormone receptor-positive, HER2-negative metastatic breast cancer (Rencuzogullari et al., 2020; Shah et al., 2018). These substances competitively bind the ATP-binding pocket of CDK4/6, inhibit Rb phosphorylation, and induce G1 cell cycle arrest. Combination strategies integrating CDK6 inhibitors with endocrine therapy, chemotherapy, or immunotherapy have further enhanced therapeutic efficacy and addressed resistance mechanisms. CDK6 disruption prolonged the G1 phase and inhibited S-phase entry in these cells. G1-phase lengthening has been shown to induce premature differentiation in neuroepithelial cells, explaining the decreased proliferation associated with CDK6 disruption (Pavani et al., 2016; Spring et al., 2020).

Natural products have also gained interest as potential modulators of CDK6 activity (Figure 2). Bioactive phytochemicals that modulate cell cycle and apoptosis-related pathways, such as flavonoids (e.g., quercetin, fisetin), resveratrol, curcumin, sulforaphane, and monoterpenes like limonene, exhibit anti-proliferative properties (Srivastava & Saxena, 2025). These compounds affect cancer-associated signaling networks, including RB-E2F, PI3K/Akt/mTOR, NF-κB, and MAPK pathways, and may contribute to CDK6 inhibition either directly or indirectly (Kim et al., 2013; de Figueiredo et al., 2015; Sa & Das, 2008; Spring et al., 2020).

Limonene, a naturally occurring monocyclic monoterpene abundant in citrus oils, promotes the GST (Glutathione S-transferase) system in the liver and small bowel, which helps in eliminating carcinogens (Sun, 2007). Limonene 1,2-diol has been reported to inhibit tumor growth through inhibition of p21-dependent signaling, induce apoptosis via the induction of the transforming growth factor beta-signaling pathway, inhibit post-translational modification of signal transduction proteins, result in G1 cell cycle arrest, and modulate genes associated with cell cycle progression and apoptosis (Sun, 2007).

Collectively, CDK6 occupies a central position at the intersection of cell cycle control, oncogenic signaling, and immune regulation. Its structural features, multilayered regulatory mechanisms, and proven druggability highlight its significance as both a mechanistic driver of tumorigenesis and a compelling therapeutic target. Continued exploration of CDK6 biology and inhibition strategies, synthetic and natural, holds substantial promise for advancing precision oncology.

2. MATERIALS AND METHODS

2.1. Chemicals and reagents

The expression vector pET-28a(+) and *Escherichia coli* BL21 (DE3) competent cells were procured from Qiagen, while *E. coli* DH5α cells were obtained from Invitrogen. Analytical-grade reagents,

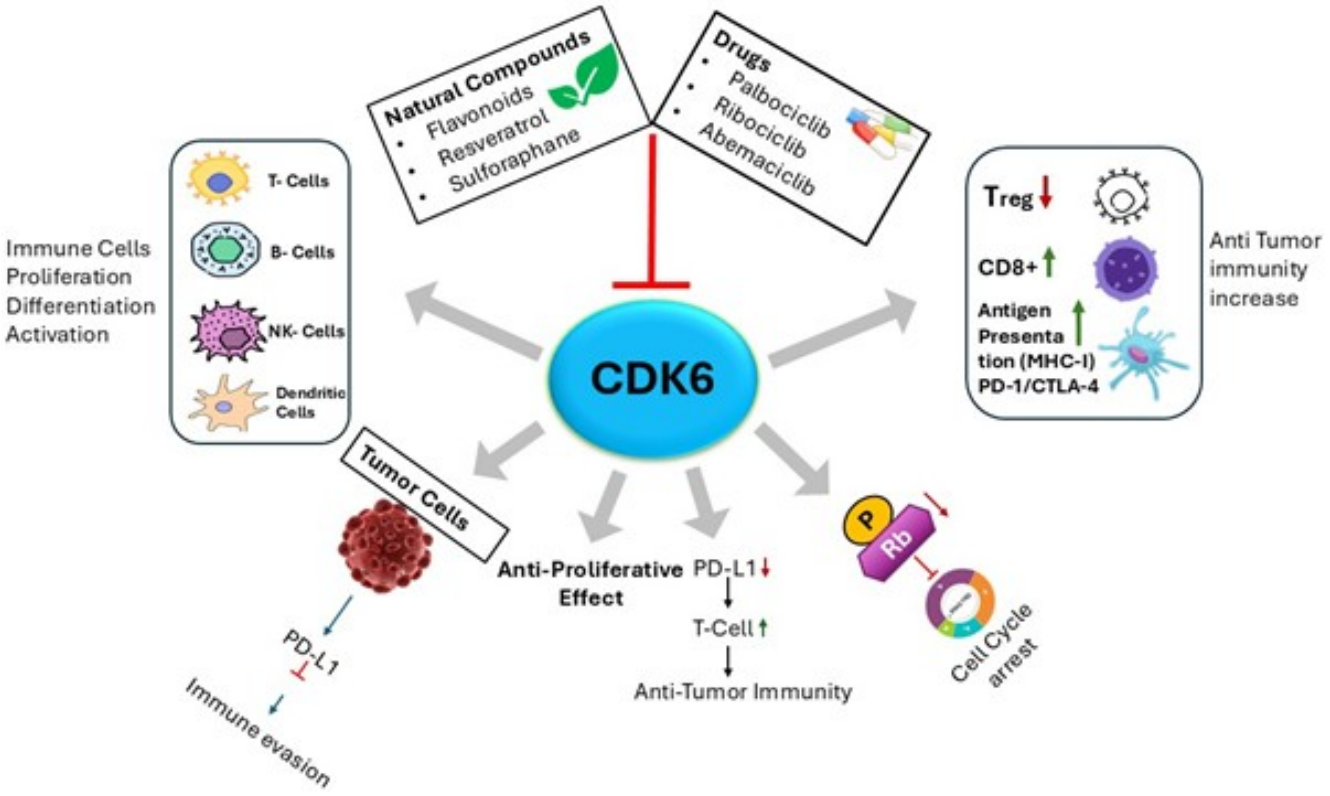

Figure 2. The diagram illustrates the central role of CDK6 in coordinating tumor cell proliferation and immune regulation. CDK6 promotes cell cycle progression by phosphorylating Rb, facilitating tumor growth and immune evasion via PD-L1 regulation. Inhibition of CDK6 by approved inhibitors or bioactive natural compounds induces cell-cycle arrest, reduces PD-L1 expression, and suppresses tumor growth. In parallel, CDK6 modulation influences immune cell proliferation, differentiation, and activation, including those of T cells, B cells, NK cells, and dendritic cells. Therapeutic targeting of CDK6 decreases regulatory T cells (Tregs) while enhancing $CD8^+$ T-cell responses and antigen presentation (MHC-I), thereby strengthening anti-tumor immunity.

including sodium chloride (NaCl), ethylenediaminetetraacetic acid (EDTA), and other routine chemicals, were purchased from Merck (India). Luria–Bertani (LB) broth was obtained from Merck (Darmstadt, Germany). Kanamycin and isopropyl-β-D-thiogalactopyranoside (IPTG) were sourced from Sigma-Aldrich (St. Louis, MO, USA). Nickel–nitrilotriacetic acid (Ni–NTA) affinity chromatography columns and Ni–NTA agarose beads were acquired from Bio-Rad and Qiagen (QIAexpress), respectively. Limonene used in this study was purchased from Sigma-Aldrich (USA).

2.2. Molecular docking

Molecular docking was performed to investigate the binding interactions between Conformer3D_COMPOUND_CID_22311 (limonene) and the crystal structure of CDK6 (PDB ID: 3NUP). Docking simulations were conducted using InstaDock, an automated platform for structure-based virtual screening (Mohammad et al., 2021). Binding affinity calculations were carried out using QuickVina-W (Hassan et al., 2017), a modified version of AutoDock Vina (Trott & Olson, 2010) that integrates empirical and knowledge-based scoring functions. A blind docking approach was employed to allow unbiased exploration of potential ligand-binding sites across the protein surface. The predicted binding free energy (ΔG, kcal mol^{-1}) obtained from docking was used to calculate the inhibitory constant ($K_{i,\mathrm{pred}}$) and pK_i values according to the following thermodynamic relationships:

$$\Delta G = RT \ln K_{i,\mathrm{pred}} \tag{1}$$

$$K_{i,\mathrm{pred}} = e^{(\Delta G/RT)} \tag{2}$$

$$pK_i = -\log K_{i,\mathrm{pred}} \tag{3}$$

where ΔG represents the docking-derived binding free energy, R is the universal gas constant (1.98 cal mol^{-1} K^{-1}), T is the temperature (298.15 K), and $K_{i,\mathrm{pred}}$ is the predicted inhibition constant (Shityakov & Foerster, 2014).

To further evaluate ligand binding efficiency, ligand efficiency (LE) was calculated using:

$$LE = -\frac{\Delta G}{N} \tag{4}$$

where LE denotes ligand efficiency (kcal mol^{-1} per non-hydrogen atom), ΔG is the binding free energy, and N corresponds to the number of non-hydrogen atoms in the ligand. This parameter provides a normalized assessment of binding strength relative to molecular size (Hopkins et al., 2004).

2.3. Plasmid isolation

The overnight bacterial culture was pelleted by centrifugation at 6000 rpm for 5 minutes at room temperature, then resuspended in the resuspension buffer. Lysis was performed to release cellular contents, including plasmid DNA, using the lysis buffer. Proteins

were then digested using proteinase K. Purification of the plasmid was done using a phenol-chloroform extraction kit. Finally, the concentration and purity of plasmid DNA were checked using Nanodrop at 260 nm. Purified bands of isolated plasmid were also confirmed using agarose gel electrophoresis (Ausubel et al., 1992).

2.4. Agarose gel electrophoresis

A 0.8% agarose gel was prepared by adding TAE buffer and heating in a microwave. EtBr was added to the cooled gel solution, and then the cooled gel was poured into the gel tray. Gel was allowed to solidify for about 20 min. Samples were prepared by adding loading dye (bromophenol blue) to the isolated plasmid DNA, and loading the samples into the wells after removing the comb. The tank was filled with TAE buffer, and the leads were connected to the power supply. After applying a constant voltage of 100–150 V for about 45–60 minutes, the gel was removed from the gel box, placed on a UV transilluminator, and visualized using a gel documentation system.

2.5. Competent cell preparation and transformation

A single colony was inoculated into LB broth containing kanamycin and incubated overnight at 37 °C, then transferred to a larger volume of fresh LB broth and incubated until the OD reached 0.4–0.6 at 600 nm. Metabolic activity was reduced by cooling the culture on ice for 15–30 minutes. Culture was centrifuged, and the supernatant was discarded. Pellet was resuspended in ice-cold 10% glycerol solution. Competent cells formed were aliquoted in microcentrifuge tubes and stored at −80 °C (Russell & Sambrook, 2001).

The recombinant plasmid construct pET-28a(+) harboring the CDK6 gene was transformed into *Escherichia coli* BL21 (DE3) competent cells using the heat-shock method. Briefly, chemically competent BL21 (DE3) cells were thawed on ice, and 50–100 ng of plasmid DNA was gently mixed with the cells. The mixture was incubated on ice for 20 min to facilitate DNA adsorption. Subsequently, cells were subjected to a heat shock at 42 °C for 90 s, followed by immediate ice incubation for 5 min to stabilize the membranes. Thereafter, 900 μL of Luria–Bertani (LB) broth was added, and the cells were allowed to recover at 37 °C with shaking at 220 rpm for 1 h. The transformed cells were then spread onto LB agar plates supplemented with kanamycin and incubated overnight (12–16 h) at 37 °C to allow colony formation (Yousuf et al., 2022).

2.6. Expression and purification

The full-length CDK6 gene (981 nucleotides) was cloned into the pET-28a(+) expression vector and sequence-verified prior to protein expression. The recombinant plasmid was transformed into *Escherichia coli* BL21 (DE3) cells for heterologous protein production. Transformed cells were cultured in LB medium containing kanamycin at 37 °C until the desired optical density was reached, then induced with 0.25 mM isopropyl-β-D-thiogalactopyranoside (IPTG). After induction, cells were harvested by centrifugation and resuspended in lysis buffer (25 mM Tris–HCl, pH 8.0, 200 mM NaCl, 1 mM DTT, and 10 mM PMSF). Cell disruption was performed by sonication on ice, and the lysate was centrifuged at 9,000 rpm for 20 min at 4 °C to separate soluble and insoluble fractions. The pellet containing inclusion bodies was collected and washed three times with Milli-Q water to remove impurities.

The inclusion bodies were subsequently solubilized in solubilization buffer (25 mM Tris–HCl, 200 mM NaCl, and 0.5% sarcosine) and loaded onto a pre-equilibrated Ni–NTA affinity chromatography column for purification. After binding, the column was washed to remove non-specifically bound proteins, and recombinant CDK6 was eluted using elution buffer containing 150 mM imidazole (25 mM Tris–HCl, pH 8.0, 200 mM NaCl). Protein purity and molecular weight were analyzed using 12% SDS–PAGE (Yousuf et al., 2020).

2.7. Kinase inhibition assay

The inhibitory effect of limonene on recombinant CDK6 was evaluated using a malachite green–based ATPase assay. The reaction mixture (final volume: 50 μL) contained purified CDK6 (1 μM) and freshly prepared ATP (200 μM). Increasing concentrations of limonene were added to assess dose-dependent inhibition. The reaction mixtures were incubated at 37 °C for 45 min to allow ATP hydrolysis. The reaction was terminated by adding 100 μL of malachite green reagent, followed by incubation at room temperature for 15–20 min to enable color development resulting from inorganic phosphate release. Absorbance was measured at 600 nm using a microplate ELISA reader in a 96-well format. Enzyme activity was calculated based on phosphate release, and percentage inhibition was determined relative to control reactions lacking inhibitor (Voura et al., 2019).

2.8. Fluorescence measurement

The interaction between limonene and purified recombinant CDK6 was investigated using intrinsic fluorescence spectroscopy by monitoring changes in the emission spectrum of CDK6 upon ligand titration (Jameel et al., 2017). Fluorescence measurements were performed using a JASCO spectrofluorometer (Model FP-6200). Titration experiments were conducted by progressively increasing the limonene concentration, and each measurement was performed in triplicate to ensure reproducibility. Changes in fluorescence intensity were recorded and analyzed to determine binding parameters. The binding constant (Ka), number of binding sites (n), and associated thermodynamic parameters were calculated from fluorescence quenching data using the Stern–Volmer equation. Analysis of the quenching behavior enabled characterization of the binding affinity and interaction mechanism between limonene and CDK6 (Shamsi et al., 2020).

3. RESULTS

3.1. Molecular docking

Docking analysis of Conformer3D_COMPOUND_CID_22311 (limonene) against the CDK6 crystal structure (PDB ID: 3NUP) revealed a predicted binding free energy (ΔG) of −6.3 kcal mol^{-1}. The corresponding calculated pK_i value was 4.62, indicating moderate binding affinity toward the target protein. The ligand efficiency (LE) was determined to be 0.63 kcal mol^{-1} per non-hydrogen atom, suggesting favorable binding energy relative to molecular size (Figure 3).

Comprehensive interaction profiling of all generated docked conformations was performed to examine the binding orientation and molecular interactions within the 3NUP binding pocket (Figure 4). Analysis of the best-ranked pose revealed that the ligand occupies the active-site cavity and establishes stabilizing interactions with key amino acid residues, thereby contributing to its predicted binding affinity.

3.2. Protein expression and purification

Plasmid isolated using the QIAprep® Spin Miniprep Kit was checked for purity and concentration using a Nanodrop, which showed a purity of about 1.8 (A260/280), and digested bands were

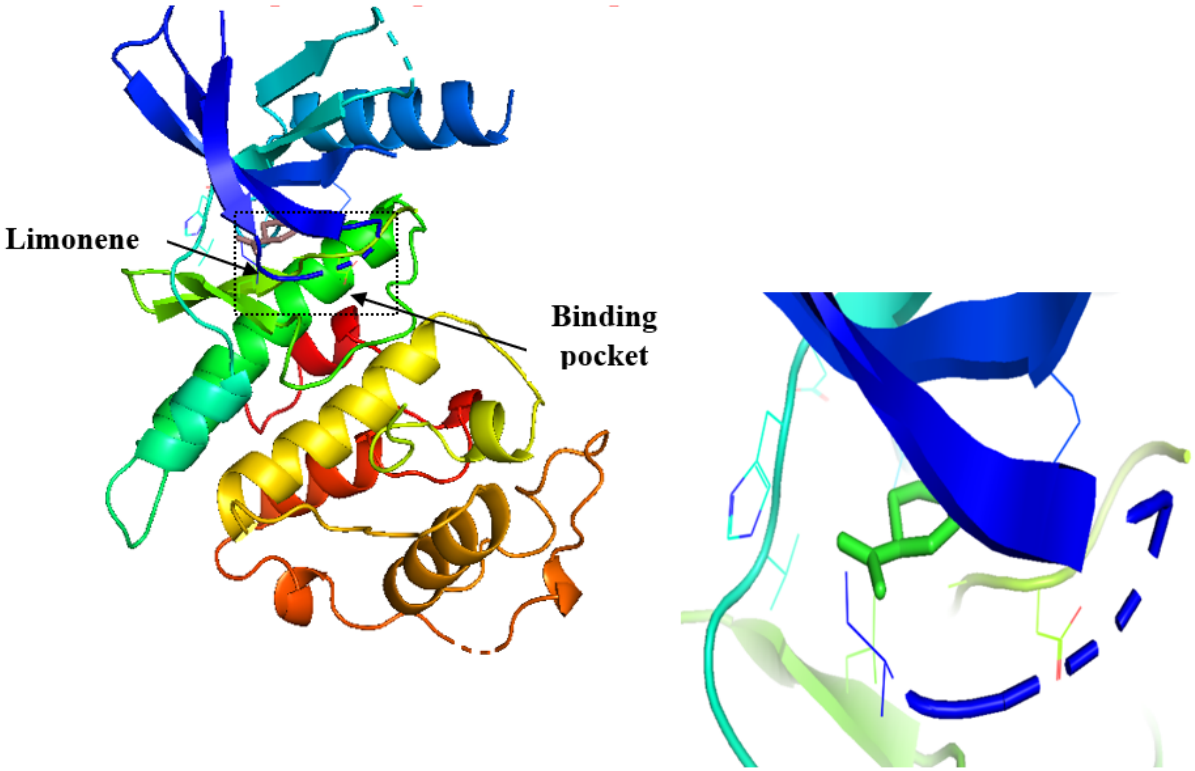

Figure 3. Representation of the binding mode of limonene to CDK6. (A) Cartoon representation of CDK6 in complex with docked limonene. (B) Zoomed interaction of limonene with the active-site pocket residues of CDK6.

visualized by running an agarose gel, which showed clear bands for nicked, linear, and supercoiled forms of DNA (Figure 5). The confirmed pET28a+ plasmid was successfully transformed into *E. coli* strain BL21 (DE3). Colonies appeared after incubation with kanamycin at 50 μg/ml for 12–16 hours at 37 °C (Figure 5). Recombinant CDK6 protein was expressed at 37 °C by inducing with 0.25 mM IPTG. Purified CDK6 protein was obtained by Ni–NTA affinity chromatography, confirmed by running SDS–PAGE (Figure 5).

3.3. Fluorescence binding studies

Intrinsic fluorescence spectroscopy was employed to evaluate the interaction between limonene and recombinant CDK6. Progressive addition of limonene led to a marked decrease in the intrinsic fluorescence intensity of CDK6, indicating effective quenching of the protein's fluorescence (Figure 6). This observation suggests that ligand binding alters the local microenvironment surrounding aromatic fluorophores (primarily tryptophan residues), thereby affecting emission characteristics. The fluorescence quenching data were analyzed using both the Stern–Volmer and modified Stern–Volmer equations to determine the quenching mechanism and binding parameters. The Stern–Volmer plot demonstrated a concentration-dependent quenching profile, supporting the formation of a protein–ligand complex.

Binding parameters derived from the modified Stern–Volmer plot revealed a binding constant (Ka) of 4.1×10^6 M^{-1}, indicative of strong affinity between limonene and CDK6. The slope of the modified plot further provided the number of binding sites (n), suggesting a defined binding interaction. The high binding constant obtained from fluorescence analysis is consistent with the molecular docking results, collectively supporting a stable and favorable interaction between limonene and CDK6.

3.4. Kinase inhibition assay

The inhibitory effect of limonene on recombinant CDK6 kinase activity was evaluated in a dose-dependent manner. Increasing concentrations of limonene resulted in a progressive reduction in CDK6 enzymatic activity. The observed decrease in kinase activity demonstrates that limonene effectively suppresses CDK6 function, supporting its potential role as a kinase inhibitor. These findings are consistent with both the molecular docking predictions and fluorescence binding studies, collectively indicating a stable interaction that translates into functional inhibition of the enzyme.

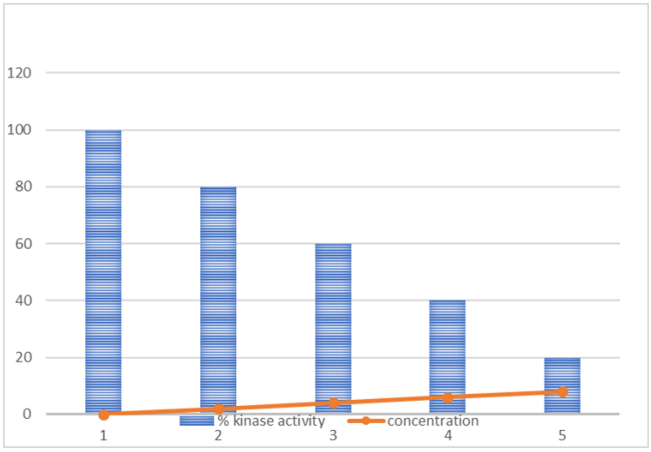

Figure 7. Graph representing enzyme activity versus ligand (limonene) concentration in the kinase inhibition assay.

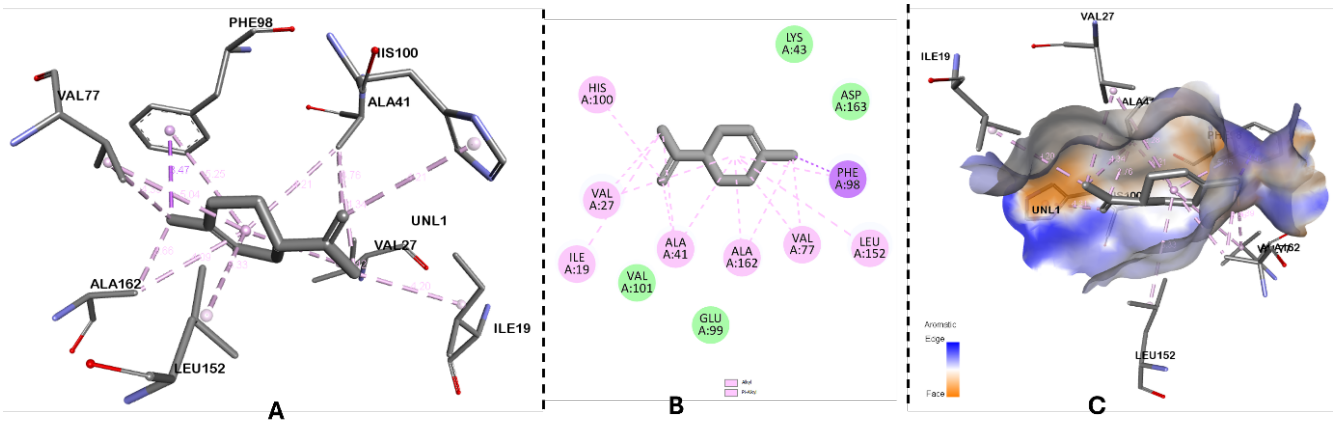

Figure 4. Molecular docking analysis of limonene with CDK6 active site. (A) Three-dimensional binding pose of limonene in the CDK6 catalytic pocket, showing key residues involved in hydrophobic stabilization. (B) Two-dimensional map showing hydrogen bonding and π–alkyl/alkyl interactions between limonene and active-site amino acids. (C) Surface representation of the CDK6 binding pocket illustrating favourable shape complementarity and hydrophobic interactions.

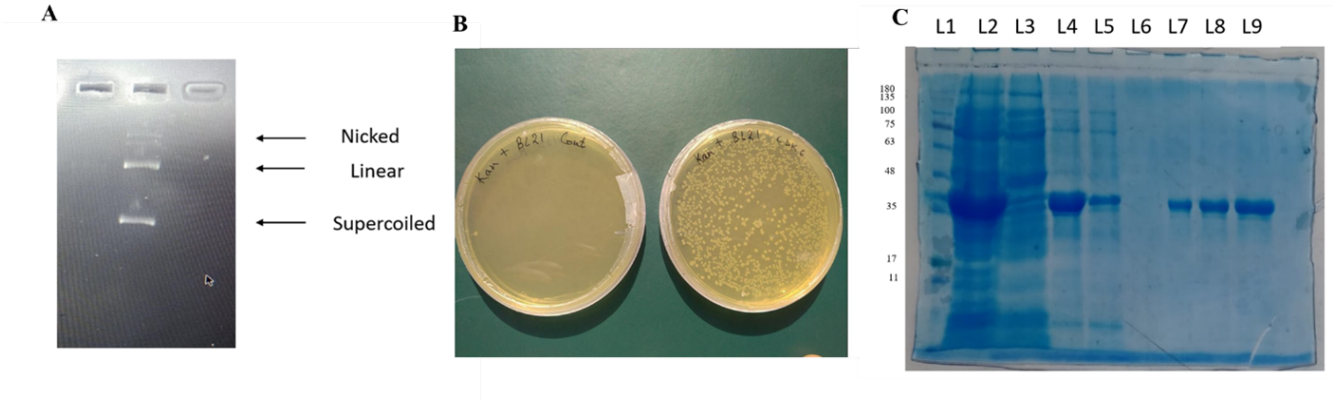

Figure 5. (A) Restriction digestion of the isolated plasmid, lane 1 showing the nicked, linear, and supercoiled forms of DNA. (B) Transformed *E. coli* BL21 colonies on an LB agar plate. (C) Purified CDK6 protein, eluted with 150 mM imidazole-containing elution buffer (lanes 7–9).

4. DISCUSSION

CDKs control cell division, which is especially important in cancer. CDK4 and CDK6 are activated by D-cyclins. As a result, CDK4 and CDK6 regulate the G1-to-S transition in the cell cycle. CDK6 plays an important part in cell-cycle regulation. CDK4/6 inhibitors suppress Rb phosphorylation and arrest the G1 phase of the cell cycle, thereby reducing tumour progression. In many cancers, the CDK4/6–INK4–Rb signalling pathway is dysregulated. CDK4/6 has emerged as a possible therapeutic target (Fontanella et al., 2022). These CDK4/6 inhibitors may become beneficial for tumour therapy after two decades of scientific development. Cyclin-dependent kinases 4 and 6 (CDK4/6) play a central role in regulating cell-cycle progression through the G1–S phase transition, making them critical drivers of uncontrolled proliferation in cancer. Pharmacological inhibition of CDK4/6 has demonstrated potent anti-proliferative effects by inducing cell-cycle arrest and promoting senescence in tumor cells. Consequently, CDK4/6 has emerged as a validated therapeutic target across multiple malignancies (Zhu & Zhu, 2023).

Several selective CDK4/6 inhibitors have received clinical approval for the treatment of hormone receptor–positive breast cancer, demonstrating favorable safety profiles and significant therapeutic benefit. Notably, agents such as Palbociclib, Ribociclib, and Abemaciclib have substantially improved progression-free survival when administered in combination with endocrine therapy. These findings underscore the clinical value of combination strategies, as CDK4/6 inhibition enhances the efficacy of other therapeutic agents and may help overcome resistance mechanisms (Illia et al., 2026).

Despite these advances, variability in patient response highlights the need for predictive biomarkers to identify individuals most likely to benefit from CDK4/6-targeted therapies. Furthermore, expanding the application of CDK4/6 inhibitors to additional tumor types requires comprehensive preclinical validation and well-designed large-scale clinical trials. Continued research focusing on combination regimens, resistance pathways, and molecular determinants of response will be essential to fully exploit the therapeutic potential of CDK4/6 inhibition in cancer management (Sun et al., 2025).

5. CONCLUSION

Elevated CDK6 expression has been strongly correlated with the progression and poor prognosis of multiple cancer types, underscoring its importance as a therapeutic target for the development of selective small-molecule inhibitors.

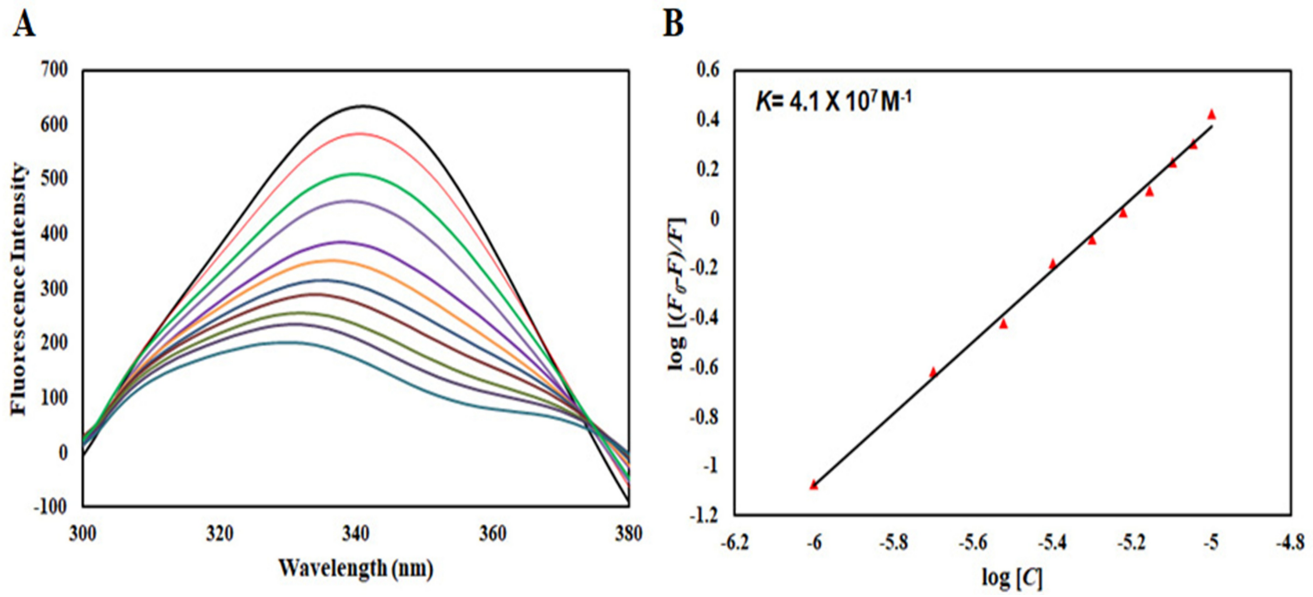

Figure 6. Fluorescence binding analysis of limonene with CDK6. (A) Intrinsic fluorescence emission spectra of CDK6 recorded in the presence of increasing concentrations of limonene. The excitation wavelength (λ_{ex}) was fixed at 280 nm, and emission spectra were collected over the range of 300–400 nm. A progressive decrease in fluorescence intensity was observed upon ligand titration, indicating quenching of CDK6 fluorescence. (B) Modified Stern–Volmer plot derived from fluorescence quenching data of CDK6 in the presence of limonene. The linear fitting of the plot was used to determine the binding constant (Ka) and the number of binding sites (n), reflecting the strength and stoichiometry of the protein–ligand interaction.

Natural compounds continue to represent a valuable reservoir of structurally diverse bioactive molecules with potential applications in oncology. In the present study, limonene was identified as a promising CDK6 inhibitor through integrated *in silico*, biophysical, and enzymatic analyses. The observed binding affinity and functional suppression of CDK6 activity suggest that limonene may contribute to its anticancer effects, at least in part, by modulating cell-cycle regulatory pathways. This mechanistic insight provides a novel perspective on the anticancer potential of limonene. Importantly, the relatively simple chemical scaffold of limonene offers opportunities for rational structural modification to enhance potency, selectivity, and drug-like properties. Structure-guided optimization strategies may facilitate the development of limonene-derived analogues as preclinical leads targeting CDK6. Further cellular and *in vivo* investigations are warranted to validate its therapeutic potential and to advance translational applications.

6. Funding

This work received no funding.

7. Acknowledgments

Zulfareen acknowledges Jamia Millia Islamia for providing the Non-NET fellowship.

8. Conflicts of Interest

The authors declare no conflicts of interest.

9. Data Availability Statement

All data generated or analyzed during this study are included in this manuscript.

10. Declaration on the Use of Artificial Intelligence (AI) Tools

The authors declare that artificial intelligence (AI) tools, specifically ChatGPT (OpenAI), were used solely to refine the language, improve grammar, and enhance the clarity of the manuscript. The AI tool was not used to generate scientific content, analyze data, interpret results, or draw scientific conclusions.

REFERENCES

Ausubel, F. M., Brent, R., Kingston, R. E., et al. 1992, Short Protocols in Molecular Biology (New York), 28764–28773

Bachs, O., Gallastegui, E., Orlando, S., et al. 2018, Oncotarget, 9, 26259

Classon, M., & Harlow, E. 2002, Nature Reviews Cancer, 2, 910

de Figueiredo, S. M., Binda, N. S., Nogueira-Machado, J. A., Vieira-Filho, S. A., & Caligiorne, R. B. 2015, Recent Patents on Endocrine, Metabolic & Immune Drug Discovery, 9, 24

Fontanella, C., Giorgi, C. A., Russo, S., et al. 2022, Critical Reviews in Oncology/Hematology, 180, 103848, doi: 10.1016/j.critrevonc.2022.103848

Garzon, R., Marcucci, G., & Croce, C. M. 2010, Nature Reviews Drug Discovery, 9, 775

Hallett, S. T., Pastok, M. W., Morgan, R. M. L., et al. 2017, Cell Reports, 21, 1386

Hanahan, D., & Weinberg, R. A. 2011, Cell, 144, 646

Hassan, N. M., Alhossary, A. A., Mu, Y., & Kwoh, C.-K. 2017, Scientific Reports, 7, 15451

Hopkins, A. L., Groom, C. R., & Alex, A. 2004, Drug Discovery Today, 9, 430

Illia, M. F., Colucci, G., Rodriguez Mignola, A., et al. 2026, Translational Breast Cancer Research, 7, 7, doi: 10.21037/tbcr-25-46

Jameel, E., Naz, H., Khan, P., et al. 2017, Chemical Biology & Drug Design, 89, 741
Kim, J.-A., Kim, D. H., Hossain, M. A., et al. 2013, International Journal of Oncology, 44, 473
Li, Y., Zhang, J., Gao, W., et al. 2015, International Journal of Molecular Sciences, 16, 9314
Malumbres, M. 2014, Genome Biology, 15, 122
Mohammad, T., Mathur, Y., & Hassan, M. I. 2021, Briefings in Bioinformatics, 22, bbaa279
Nebenfuehr, S., Kollmann, K., & Sexl, V. 2020, International Journal of Cancer, 147, 2988
O'Sullivan, C. C. 2026, Cancers, 18, doi: 10.3390/cancers18030533
Pavani, R. S., da Silva, M. S., Fernandes, C. A. H., et al. 2016, PLoS Neglected Tropical Diseases, 10, e0005181
Petroni, G., Formenti, S. C., Chen-Kiang, S., & Galluzzi, L. 2020, Nature Reviews Immunology, 20, 669
Rencuzogullari, O., Yerlikaya, P. O., Gurkan, A. C., Arisan, E. D., & Telci, D. 2020, Journal of Cellular Biochemistry, 121, 508
Russell, D. W., & Sambrook, J. 2001, Molecular Cloning: A Laboratory Manual (Cold Spring Harbor, NY: Cold Spring Harbor Laboratory)
Russo, A. A., Tong, L., Lee, J.-O., Jeffrey, P. D., & Pavletich, N. P. 1998, Nature, 395, 237
Sa, G., & Das, T. 2008, Cell Division, 3, 14
Shah, A., Bloomquist, E., Tang, S., et al. 2018, Clinical Cancer Research, 24, 2999
Shamsi, A., Anwar, S., Mohammad, T., et al. 2020, Biomolecules, 10, 789
Sherr, C., Beach, D., & Shapiro, G. 2016, Cancer Discovery, 6, 353
Shityakov, S., & Foerster, C. 2014, Advances and Applications in Bioinformatics and Chemistry, 1
Sielecki, T. M., Boylan, J. F., Benfield, P. A., & Trainor, G. L. 2000, Journal of Medicinal Chemistry, 43, 1
Spring, L. M., Wander, S. A., Andre, F., et al. 2020, The Lancet, 395, 817
Srivastava, N., & Saxena, A. K. 2025, Current Medicinal Chemistry, 32, 7512, doi: 10.2174/0109298673331685241205180307
Sun, J. 2007, Alternative Medicine Review, 12, 259
Sun, Y., Zhao, Y., Yu, X., Qi, Y., & Dai, X. 2025, Discover Oncology, 17, 138, doi: 10.1007/s12672-025-04269-2
Tigan, A., Bellutti, F., Kollmann, K., Tebb, G., & Sexl, V. 2016, Oncogene, 35, 3083
Trott, O., & Olson, A. J. 2010, Journal of Computational Chemistry, 31, 455
Voura, M., Khan, P., Thysiadis, S., et al. 2019, Scientific Reports, 9, 1676
Yousuf, M., Alam, M., Shamsi, A., et al. 2022, International Journal of Biological Macromolecules, 218, 394, doi: 10.1016/j.ijbiomac.2022.07.156
Yousuf, M., Shamsi, A., Khan, P., et al. 2020, International Journal of Molecular Sciences, 21, 3526
Zhu, Z., & Zhu, Q. 2023, Frontiers in Pharmacology, 14, 1212986, doi: 10.3389/fphar.2023.1212986